Localized-density-matrix, segment-molecular-orbitals and poly(p–phenylenevinylene) aggregates

Satoshi Yokojima, XiuJun Wang, DongHao Zhou, and GuanHua Chen

Citation: The Journal of Chemical Physics **111**, 10444 (1999);
View online: https://doi.org/10.1063/1.480432
View Table of Contents: http://aip.scitation.org/toc/jcp/111/23
Published by the American Institute of Physics

Localized-density-matrix, segment-molecular-orbitals and poly(*p*-phenylenevinylene) aggregates

Satoshi Yokojima, XiuJun Wang, DongHao Zhou, and GuanHua Chen
Department of Chemistry, The University of Hong Kong, Pokfulam Road, Hong Kong

(Received 8 July 1999; accepted 16 September 1999)

The segment-molecular-orbital representation is developed and incorporated into the recently developed linear-scaling localized-density-matrix method. The entire system is divided into many segments, and the molecular orbitals of all segments form the basis functions of the segment-molecular-orbital representation. Introduction of different cutoff lengths for different segment-molecular-orbitals leads to a drastic reduction of the computational cost. As a result, the modified localized-density-matrix method is employed to investigate the optical responses of large Poly(*p*-phenylenevinylene) aggregates. In particular, the interchain excitations are studied. The complete neglect of differential overlap in spectroscopy hamiltonian is employed in the calculation.
 [S0021-9606(99)30446-3]

I. INTRODUCTION

As researchers are interested in increasingly large and complex systems, the development of linear-scaling methods has become an active research area of quantum chemistry.[1–20] Several linear scaling methods have been developed to calculate electronic ground states.[1–20] However, linear-scaling calculation had been a much more difficult task for the excited states until recently. The first linear-scaling calculation with explicit electron–electron Coulomb interaction for excited state properties was carried successfully to determine the linear optical response of large polyacetylene oligomers.[21,22] The Pariser–Parr–Pople (PPP) Hamiltonian[23–25] was employed in the calculation. The new method, the localized-density-matrix (LDM) method, has been applied to carbon nanotubes, and generalized to include the complete neglect of differential overlap in spectroscopy (CNDO/S)[26] and MNDO-Parametric Method 3 (PM3)[27] Hamiltonians[28] and nonorthonormal basis set.[29] Based on a similar idea, the LDM method has been modified to carry a linear-scaling calculation for the ground state.[30,31] The largest linear-scaling calculation for excited state properties has been performed for a polyacetylene oligomer containing 33 000 carbon atoms by employing the PPP Hamiltonian.[32]

Compared to the PPP Hamiltonian where only the π orbitals are considered, the LDM calculation employing the semiempirical Hamiltonians like CNDO/S or PM3 are computationally more demanding since all valence electrons are included explicitly. To overcome this difficulty, we develop the segment-molecular-orbital (SMO) representation for the LDM method. A SMO is a molecular orbital (MO) spanned over a segment of a molecule. It is obtained by solving for the Hartree–Fock molecular orbitals (HFMOs) of the segment. To employ the SMO representation in the LDM calculation, a local transformation from the atomic orbitals (AOs) to SMOs is required. Since the density matrices corresponding to the low energy orbitals are well localized, much shorter cutoff lengths may then be introduced for these orbitals.

Conjugated polymers have been of great research interests. Important progress is being made towards the commercialization of light emitting diode (LED). However, many aspects of the photoexcitation mechanism remain controversial. One of the major debates has been the characteristics of photoexcitations: whether the excitations are intrachain or interchain.[33–50] Poly(*p*-phenylenevinylene) (PPV) is the most widely studied luminescent polymer. Its thin film has been used in the fabrication of the LED.[51,52] We choose it to investigate the nature of photoexcitations.

Because of the sizes and complexities of PPV and its derivatives, most theoretical works have been limited to single or double oligomers. The LDM method has been applied to very large systems,[21,22,29,32] and the incorporation of the SMO representation is expected to reduce the computational cost further. In this work, we develop the LDM method with the SMO representation (LDM/SMO) to calculate the linear response of large PPV aggregates and to examine the characters of different photoexcitations. In Sec. II we describe our method including the model, the SMO representation and the procedure of the LDM/SMO calculation. In Sec. III the results of our calculation are presented, and emphasis is given to the comparison between the interchain and intrachain excitations. Finally, the discussion and conclusion are given in Sec. IV.

II. METHOD

A. Model

We use the CNDO/S Hamiltonian to describe the valence electrons in PPV aggregates. In the presence of an external electric field $\mathcal{E}(t)$, the total Hamiltonian is given by the following expression:

$$H = H_{\mathrm{CNDO/S}} + H_{\mathrm{ext}}. \tag{1}$$

Here the Nishimoto–Mataga formula[53] is employed for two-electron integrals in $H_{\mathrm{CNDO/S}}$. H_{ext} describes the interaction between the electrons and the external electric field $\vec{\mathcal{E}}(t)$, the

dipole matrix elements $\vec{\mu}_{ij}$ in $H_{\rm ext}$ are evaluated using the zero differential overlap approximation.[54] Within the time-dependent Hartree–Fock (TDHF) approximation,[23,55,56] a closed nonlinear self-consistent equation of motion is yielded for the reduced single-electron density matrix $\rho(t)$,

$$i\left(\hbar\frac{d}{dt}+\gamma\right)\rho(t)=[h(t)+f(t),\rho(t)]. \tag{2}$$

Here $h(t)$ is the Fock matrix:

$$h_{nm}(t)=t_{nm}+2\,\delta_{nm}\sum_l v_{nl}\rho_{ll}(t)-v_{nm}\rho_{nm}(t), \tag{3}$$

where t_{nm} is the hopping matrix element between orbital m and n, and v_{nm} is the Coulomb repulsion between two electrons at AOs m and n, respectively. γ is a phenomenological dephasing. $f(t)$ describes the interaction between an electron and the external field $\vec{\mathcal{E}}(t)$ and $f_{ij}(t)=e\vec{\mu}_{ij}\cdot\vec{\mathcal{E}}(t)$.[23]

B. SMO

To determine the SMO representation, we need to determine the SMOs. The following procedure is adopted. First the entire system is divided into many segments, and the bonds between adjacent segments are severed. Each dangling bond is assigned two electrons. Secondly, the Hartree–Fock solution is determined for each segment by employing CNDO/S Hamiltonian. Denote respectively the Hartree–Fock molecular orbital coefficients and energy as S_{ij}^{α} and E_j^{α} for the jth MO of the segment α, where i is the index of the ith AO. Finally, all the resulting SMOs are taken as the basis functions, and transformation matrix S_{ij} from the AO representation to the SMO representation for the entire molecule is constructed as follows:

$$S_{ij}=\begin{cases} S_{ij}^{\alpha}, & i,j\in\alpha \\ 0, & i\in\alpha,\ j\in\beta\ \ (\alpha\neq\beta). \end{cases} \tag{4}$$

We denote the SMO representation by the bar. The density matrix $\overline{\rho}$, Fock matrix $\overline{h}$ and dipole matrix $\vec{\overline{\mu}}$ in the SMO representation are thus expressed as

$$\overline{\rho}_{ij}=\sum_{i_1j_1} S_{ii_1}^{\dagger}\rho_{i_1j_1}S_{j_1j},\quad \overline{h}_{ij}=\sum_{i_1j_1} S_{ii_1}^{\dagger}h_{i_1j_1}S_{j_1j},$$
$$\vec{\overline{\mu}}_{ij}=\sum_{i_1j_1} S_{ii_1}^{\dagger}\vec{\mu}_{i_1j_1}S_{j_1j}. \tag{5}$$

Note that Eq. (5) is merely a change of the representation, and thus no approximation has been made here.

Computationally, there are two advantages for employing the SMO representation for the LDM calculation.

(1) In the AO representation many orbitals have a long cutoff length for the density matrix, whereas in the SMO representation the SMOs far from the Fermi energy or chemical potential have much shorter cutoff length. By introduction of different cutoff lengths for different pairs of SMOs, we may reduce drastically the number of density matrix elements to be considered explicitly, and consequently save much of the computational time.

(2) Those SMOs far away from the Fermi energy or chemical potential are optically inactive the visible range, and may be simply cut off from the density matrix and the equation of motion.

In our calculation we keep all SMOs but adopt different cutoff lengths for different SMO pairs, i.e., employing only the approximation 1.

C. Localized-density-matrix/segment-molecular-orbitals (LDM/SMO) method

We denote the ground state density matrix and Fock matrix by $\rho^{(0)}$ and $h^{(0)}$, respectively. The ith order of induced density matrix or Fock matrix in $\vec{\mathcal{E}}(t)$ is indicated by the superscript (i), i.e., $\delta\rho^{(i)}$ or $\delta h^{(i)}$, respectively. Thus the equation for the linear optical response of the density matrix ρ in the SMO is given by inserting $\rho=\rho^{(0)}+\delta\rho^{(1)}+\delta\rho^{(2)}+\delta\rho^{(3)}+\cdots$ into (2), retaining the first order in $\vec{\mathcal{E}}(t)$ and then transforming the equation from AO to SMO:

$$\begin{aligned} i\hbar\,\delta\dot{\overline{\rho}}_{ij}^{(1)}=&\sum_l\ (\overline{h}_{il}^{(0)}\delta\overline{\rho}_{lj}^{(1)}-\delta\overline{\rho}_{il}^{(1)}\overline{h}_{lj}^{(0)}) \\ &+\sum_l\ (\delta\overline{h}_{il}^{(1)}\delta\overline{\rho}_{lj}^{(0)}-\delta\overline{\rho}_{il}^{(0)}\delta\overline{h}_{lj}^{(1)}) \\ &+\sum_l\ e\vec{\mathcal{E}}(t)\cdot(\vec{\overline{\mu}}_{il}\overline{\rho}_{lj}^{(0)}-\overline{\rho}_{il}^{(0)}\vec{\overline{\mu}}_{lj}), \end{aligned} \tag{6}$$

where

$$\begin{aligned} \delta\overline{h}_{ij}^{(1)}=&2\sum_{i_1j_1mn} S_{ii_1}^{\dagger}S_{i_1j}v_{i_1j_1}S_{j_1m}\delta\overline{\rho}_{mn}^{(1)}S_{nj_1}^{\dagger} \\ &-\sum_{i_1j_1mn} S_{ii_1}^{\dagger}v_{i_1j_1}S_{i_1m}\delta\overline{\rho}_{mn}^{(1)}S_{nj_1}^{\dagger}S_{j_1j}. \end{aligned} \tag{7}$$

The locality of the density matrix has been investigated theoretically. A recent report[57] shows that the density matrix in the spatial representation decays exponentially,

$$\rho(\vec{r}_1,\vec{r}_2)\sim\exp(-\gamma|\vec{r}_1-\vec{r}_2|), \tag{8}$$

where γ is proportional to the energy gap for semiconductors and insulators. Therefore a critical distance for $|\vec{r}_1-\vec{r}_2|$ is introduced beyond which $\rho(\vec{r}_1,\vec{r}_2)$ is neglected. This critical distance is proportional to the inverse of the HOMO and LUMO energy gap. The above result is obtained for infinite periodic system in the weak-binding limit. We observe that different types of orbitals have different critical distances. For instance, deeply bounded orbitals or high empty orbitals rarely contribute to the optical response and thus, they have a much smaller cutoff lengths. Thus, the cutoff lengths for the ground state density matrix $\overline{\rho}^{(0)}$ in the SMO representation may be given as follows:

$$\begin{aligned} C_{ij}=&l_0\frac{E_g^{\alpha}}{t_0|E_i^{\alpha}-E^{\alpha}(i)|+E_g^{\alpha}}\frac{E_g^{\beta}}{t_0|E_j^{\beta}-E^{\beta}(j)|+E_g^{\beta}} \\ &\times\frac{\overline{E}_g}{t_0|f(E_i^{\alpha},E_j^{\beta})|+\overline{E}_g}, \end{aligned} \tag{9}$$

$$f(E_i^{\alpha},E_j^{\beta})=(E_i^{\alpha}-E^{\alpha}(i))-(E_j^{\beta}-E^{\beta}(j)). \tag{10}$$

Here C_{ij} is the cutoff length for orbitals i and j. i and j are in two different segments α and β, respectively. E_g^{α} (E_g^{β}) is half of the energy gap in α (β), and $\overline{E_g}$ is half of the averaged energy gap for the entire system. $E^{\alpha}(i)$ is the HOMO (LUMO) energy of segment α if E_i^{α} is below HOMO (above LUMO). E_j^{β} is similarly defined. We set the density matrix element $\overline{\rho}_{ij}^{(0)}=0$ in Eq. (6) when the distance between the centers of mass for α and β is longer than C_{ij}. The first term on the right-hand side (rhs) of Eq. (9), l_0, is simply the cutoff length when i and j are either HOMO or LUMO of respective segments. The second and third terms on the rhs of (9) take into account that further the orbital i or j from the HOMO or LUMO, the shorter the critical length. $|E_i^{\alpha}-E^{\alpha}(i)|$ and $|E_j^{\beta}-E^{\beta}(j)|$ measure the energy difference of i and j with respect to their segment HOMO or LUMO. t_0 is a scaling constant which is introduced to control the variation of critical length for orbitals other than segment HOMO or LUMO. The fourth term accounts for the following fact: the larger the energy difference between i and j, the smaller their critical length.

The cutoff lengths for excited states are given by replacing (l_0,t_0) with (l_1,t_1). To take into account the bonding information between segments correctly, we include all the density matrix elements $\overline{\rho}_{ij}$ for i and j which reside on the same segment or the nearest neighbors. When we take $t_0=t_1=0$, LDM/SMO method is almost equivalent to the original LDM except that the LDM/SMO method uses the distance between the centers of mass of two segments instead of the distance between two atoms. l_0 and l_1 are the same as in Refs. 21, 22, and 29.

D. Structures of PPV aggregates

We use the same bond lengths and angles of the PPV oligomer as given in Ref. 38. The C–C bond lengths along the benzene ring are set to 1.39 Å, and all the angles on the benzene are set to 120°. The C–H bond lengths are equal to 1.09 Å. The single and double bond lengths in the vinylene group are 1.44 Å and 1.33 Å, respectively. To investigate the interchain excitations we construct several PPV aggregates. Eight chain aggregates are shown in Fig. 6 where each chain is aligned along the x axis and there are 3.28 Å and 1.64 Å displacements along x direction from C to A and from B to A, respectively. The two PPV chains are either parallel (A and C) or tilted to each other with an angle 76° (A and B). The axis of B and C are displaced by (4.00 Å, 3.12 Å) and (−0.31 Å, 4.53 Å) in y–z-plane from that of A. More chains are added with the same displacement vectors and angles among them, see Figs. 6 and 10. Each PPV chain is made of multi-units and each unit consists of 8 carbon and 6 hydrogen atoms except the two ends of the chain. (The unit at either end of the chain has 8 carbon and 7 hydrogen atoms.) In the rest of this paper the notation M–N PPV represents a PPV aggregate containing N PPV chain and each chain having M units. The geometries are fixed in the calculation. There are many ways to divide a PPV chain into segments. The scheme that has been used in our calculation is shown in Fig. 1. We find that this scheme leads to high computational efficiency as well the accuracy of the calculation.

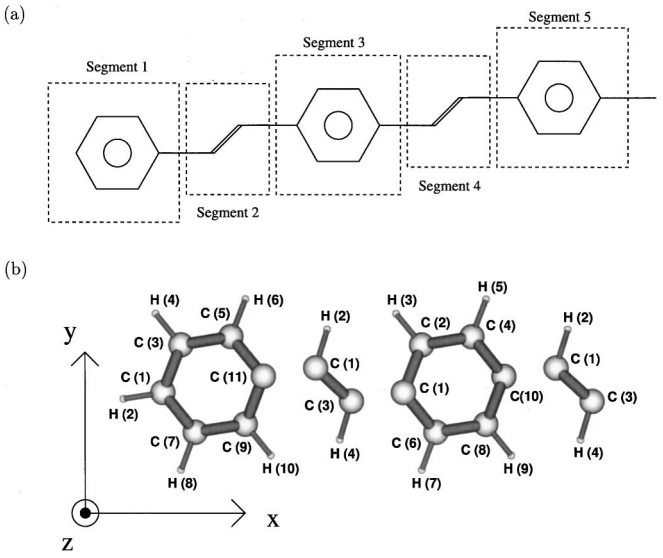

FIG. 1. Schematic diagrams for the segments of an oligomer.

III. RESULTS

The SMO representation is obtained by solving for the SMOs of each segment. The segment 2 in Fig. 1(b) has two carbon atoms [C(1) and C(3)] and two hydrogen atoms [H(2) and H(4)]. Since it has two dangling bonds, two extra electrons are added. We then solve for the Hartree–Fock MOs of the segment 2 by setting its charge to $-2e$. The resulting SMOs are listed in Table I. SMOs 5 and 7 are obviously the π orbitals. The HOMO is SMO 6 which is a σ orbital which has large components at two dangling bonds. SMO 7 is the LUMO. Here the half energy gap $E_g^2=5.09$ eV. The average HOMO and LUMO energy gap $\overline{E_g}$ is found to be 4.57 eV for 8-1 PPV.

We compare the the absorption spectra calculated by the LDM/SMO and the full TDHF for 8-1 PPV in Fig. 2. $\vec{\mathcal{E}}$ is polarized along the x axis. $t_0=t_1=0.35$, $l_0=l_1=32.0$ Å are employed in the LDM/SMO calculation. Clearly the LDM/SMO calculation yield the accurate absorption spectrum from 1.5 eV to 10 eV. Thus these parameters are employed in the subsequent calculations for 2-8 and 8-4 PPV aggregates. For smaller aggregates like 2-1 and 2-2 PPV the full TDHF method is used.

Figure 3 shows the comparison between one and two chain PPV aggregates absorption spectra with the electric field perpendicular to the plane of the chain A. The absorption spectrum of 2-2 PPV aggregates (solid line) is almost identical to the scaled absorption spectrum of 2-1 PPV oligomer (dashed line) from 8 to 10 eV in Fig. 3. A new peak appears at 4.76 eV for 2-2 PPV aggregates as compared to 2-1 oligomer. This is caused by interaction between the electrons residing separately on A and B. A clear sign of interchain effects. Further, the amplitude of the absorption spectrum from 5.5 eV to 6.5 eV is enhanced for 2-2 PPV.

TABLE I. MO coefficients and energies of SMOs for segment 2 (Fig. 1).[a]

SMO	1	2	3	4	5	6	7	8	9	10
E_i^2 (eV)	−18.75	−9.59	−1.30	−0.51	3.75	4.62	14.80	18.51	19.71	22.82
C(1)2S	0.606	−0.351	−0.073	−0.409	0.000	−0.280	0.000	−0.332	−0.221	−0.316
C(1)2P_x	0.173	0.016	−0.222	0.517	0.000	0.609	0.000	−0.282	−0.224	−0.391
C(1)2P_y	−0.106	−0.361	0.496	0.199	0.000	0.030	0.000	−0.318	−0.492	0.478
C(1)2P_z	0.000	0.000	0.000	0.000	0.707	0.000	0.707	0.000	0.000	0.000
H(2)1S	0.303	−0.496	0.446	0.160	0.000	0.224	0.000	0.458	0.399	−0.137
C(3)2S	0.606	0.351	−0.073	0.409	0.000	−0.280	0.000	0.332	−0.221	0.316
C(3)2P_x	−0.173	0.016	0.222	0.517	0.000	−0.609	0.000	−0.282	0.224	−0.391
C(3)2P_y	0.106	−0.361	−0.496	0.199	0.000	−0.030	0.000	−0.318	0.492	0.478
C(3)2P_z	0.000	0.000	0.000	0.000	0.707	0.000	−0.707	0.000	0.000	0.000
H(4)1S	0.303	0.496	0.446	−0.160	0.000	0.224	0.000	−0.458	0.399	0.137

[a]C(i)2S and C(i)2P_k stand for the carbon 2S and 2P_k ($k=x,y,z$) atomic orbitals of carbon atom i, respectively, H(i)1S denotes the hydrogen 1S atomic orbital of hydrogen atom i.

Examining the density matrices reveals the existence of the interchain excitations for the excited states, although the absorption spectra give little indication.

The ground and excited state density matrices of 2-2 PPV in Fig. 3 are shown in Figs. 4 and 5. Intensities of the ground state density matrix elements are shown by a gray logarithmic scale (see Fig. 4). Darker the color is, the larger the absolute value of matrix element is.

In Fig. 4, the first 78 orbitals correspond to chain A while others are for chain B. Figures 4(a) and 4(b) are for the same ground state but with different representation, i.e., the AO and SMO representations, respectively. In AO representation, indices are given as increasing order of segments [Fig. 1(a)] and index of atoms [Fig. 1(b)]. For carbon atoms indices are assigned with the order of 2S, 2P_x, 2P_y, and 2P_z orbital. Large square boxes and dots in Fig. 4(a) correspond to the density matrix elements related to σ and π orbitals, respectively. Thin white lines between these boxes indicate that the matrix elements of σ and π orbitals are well decoupled within the chain in spite of the fact that we have two chains in different parallel planes. We can see the coupling between σ and π orbitals in the matrix elements between chain A and B. The density matrix elements between chain A and chain B are small for the ground state.

The SMO representation [Fig. 4(b)] gives a different picture for the density matrix. Compared to Fig. 4(a) where nearly uniform density matrix is found along the band diagonal matrix within a chain, various structures appear in Fig. 4(b). To explain those structures, first let us consider an ideal case where there is no interaction among each segment. Then the ground state density matrix in the SMO representation gives diagonal matrix elements ρ_{ii} which are either 0 or 1 depending on E_i^α. (We assume here that the charges are assigned for each segment as those in the determination of SMOs.) We arrange the indices of the SMOs in an increasing order of E_i^α in segment α. As a result, the first $k/2$ diagonal elements of the ground state density matrix in each segment is 1 where k is the number of the electrons in a segment, and others are 0. However, since there is interaction among segments, the ground state density matrix will deviate from the above values. In Fig. 4(b), we find that the diagonal part has

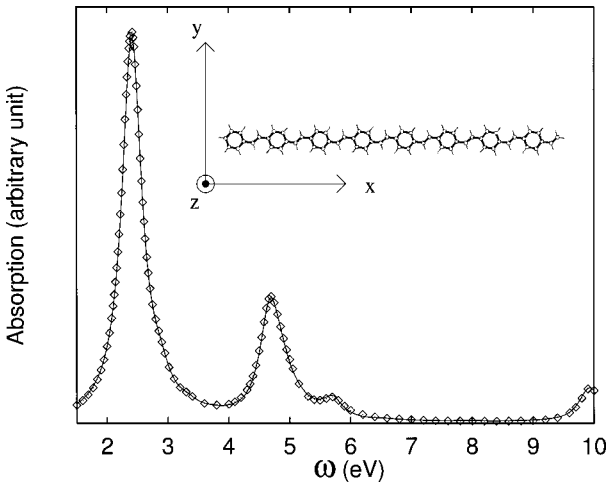

FIG. 2. Absorption spectra for 8-1 PPV oligomer. The solid line: the LDM/SMO method with $t_0=t_1=0.35$ and $l_0=l_1=32.0$ Å. Diamonds: the full TDHF calculation.

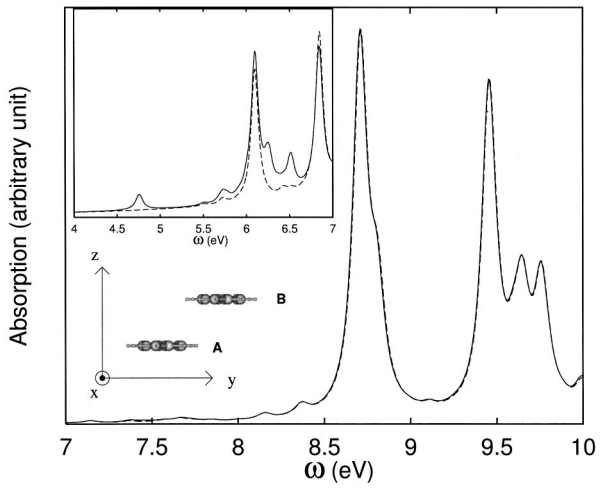

FIG. 3. Absorption spectra for PPV aggregates with the electric field perpendicular to the plane of A. The solid line: 2-2 PPV aggregates. The dashed line: 2-1 PPV oligomer A. The amplitude of the dashed line is magnified by a factor of 2. The inset shows the magnified view of the lower excited states. $\gamma=0.05$ eV.

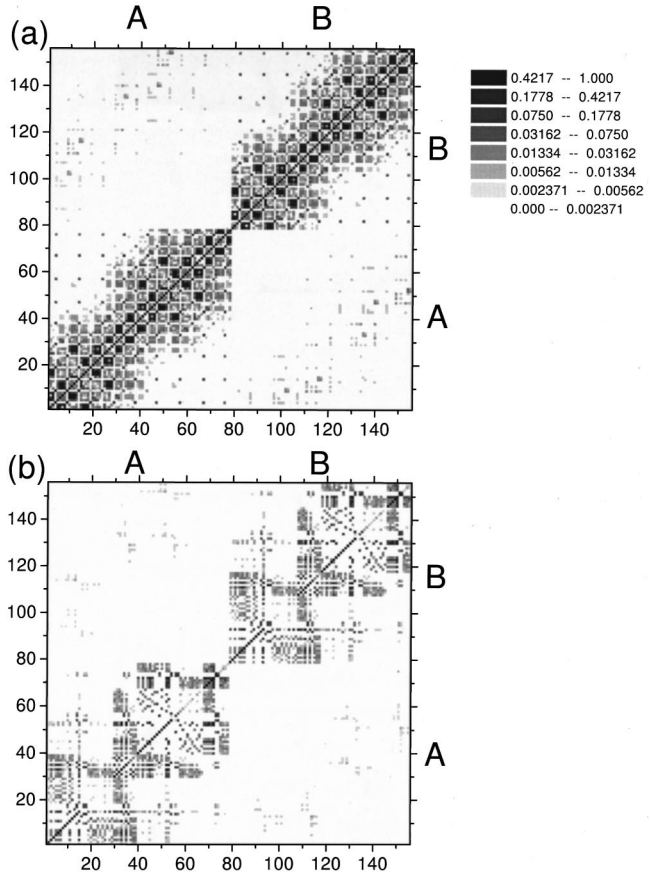

FIG. 4. Ground state density matrix for 2-2 PPV as depicted in Fig. 3. The absolute value of the matrix elements are shown by a gray logarithmic scale which is located in the right-upper corner. The matrix element is rescaled by the largest value of $\rho_{ij}^{(0)}$ or $\overline{\rho_{ij}^{(0)}}$. (a) The AO representation. (b) The SMO representation. Indices of the orbitals 1–29, 30–39, 40–67, and 68–78 belong to the segment 1, 2, 3, and 4 of A, respectively. Indices 15, 35, 54, and 73 correspond to the HOMO of its segment.

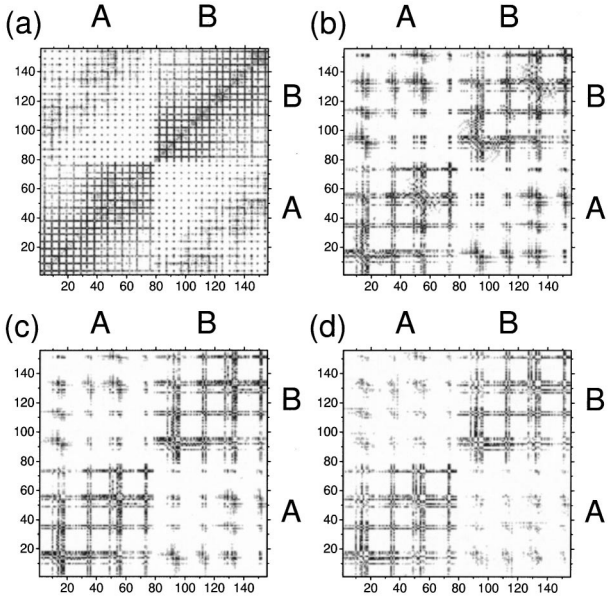

FIG. 5. Excited state density matrices $\delta\rho(\omega)$ for 2-2 PPV (in Fig. 3). The absolute vaule of the matrix elements are shown with the gray logarithmic scale in the right-upper corner of Fig. 4. The matrix elements are rescaled by the largest value of $|\delta\rho_{ij}|$ or $|\delta\overline{\rho_{ij}}|$. (a) The AO representation with $\omega = 4.76$ eV. (b) The SMO representation with $\omega = 4.76$ eV, (c) $\omega = 6.10$ eV, and (d) $\omega = 8.71$ eV.

the similar feature as just described. A vertical dark color band is observed where the abscissas of matrix elements stretch from 30 to 39 and the ordinate from 1 to 67. A similar horizontal band exists for A. This is because there are large couplings among segment 2 (from orbital 30 to 39) and its neighboring segments 1 (from orbital 1 to 29) and 3 (from orbital 40 to 67). We find the same phenomenon between segment 3 and 4 (from orbital 68 to 78). Ground state density matrix elements between non-neighboring segments are very small. In this case relatively large matrix elements appear only between the pairs of orbitals near the HOMO or LUMO in each segment. This is consistent with our assertion in Sec. II C. Note that the matrix elements among orbitals which have eigenvalues above the LUMO for any segment are small. This fact indicates that the SMO representation select mainly the orbitals relevant for the ground state, and may explain the success of the ground state linear-scaling methods.[1,14]

Figure 5 shows the excited state density matrices corresponding to three of the peaks in Fig. 3, $\omega = 4.76$ eV [Figs. 5(a) and 5(b)], 6.10 eV [Fig. 5(c)], and 8.71 eV [Fig. 5(d)]. $\delta\rho(\omega)$ is obtained by the Fourier cosine transformation:

$$\delta\rho(\omega) \equiv \int dt \cos(\omega t)\, \delta\rho(t). \tag{11}$$

The lowest excited state density matrix in the AO representation is shown in Fig. 5(a). The dark lines correspond to the matrix elements where one of the indices corresponds to a π orbital. Although π orbitals are most important to the optical response, very large σ orbital contribution to the excitation is found as well. The matrix elements between segment A and B shows the dark area from (0,100) to (60,156) because of the special arrangement of two chains. The intensities of matrix elements are very sensitive to the distance between the two orbitals. Note that the two orbitals are in different chains. Since the segment 4 in chain A is far away from the other part of B, a large white area is observed between the orbitals from 68 to 78 and the orbitals in segment B. The same excited state density matrix is transformed to the SMO representation and is given in Fig. 5(b). The figure exhibits the typical feature of the excited state density matrix in the SMO representation. The dark lines which form the kiltlike pattern correspond to the orbitals near the HOMO or LUMO of each segment. Those orbitals are responsible for the lower energy excitations and have larger critical length than others. This supports again our assertion about critical lengths in Sec. II C.

The distinctions among the excited states density matrices is clearer in the SMO representation [Figs. 5(b), 5(c), and 5(d)]. The density matrix for $\omega = 6.10$ eV [Fig. 5(c)] has minor but noticeable differences from that of $\omega = 4.76$ eV [Fig. 5(b)]. Especially the σ(below HOMO)-σ(above LUMO) matrix elements appearing in Fig. 5(b) is almost wiped out in Fig. 5(c). Although it retains the kiltlike pattern, Fig. 5(d) is quite different from Figs. 5(b) and 5(c). Surprisingly, it still

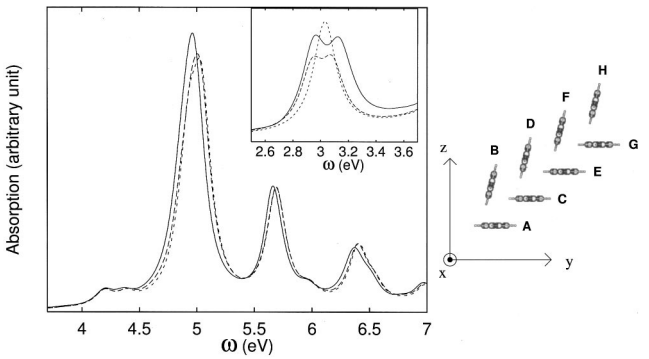

FIG. 6. Absorption spectra for 2-8 PPV aggregate. The solid line: 2-8 PPV aggregate. The dashed line: 2-2 PPV aggregate (A and B). The dotted line: 2-1 PPV oligomer (B). The dashed and dotted lines are magnified by 4 times. The inset shows the magnified view of the lower excited states. The electric field is perpendicular to the plane of A. $\gamma = 0.1$ eV.

has some matrix elements between segment A and B in spite of the fact that the absorption spectrum in Fig. 3 shows almost identical results as the absorption spectrum of one chain. Thus it is important to calculate the density matrix to investigate the interchain excitation. The small change of the absorption spectrum might be attributed to much stronger intrachain excitation which is represented by the darker strips in Fig. 5(d). These darker strips correspond to the matrix elements between segment $A-A$ or segment $B-B$ in Fig. 5(d).

The deviation of the absorption spectrum of PPV aggregates from single chain PPV oligomer is more drastic when more chains are involved. Figure 6 shows the comparison between the absorption spectra of 2-1 (chain B), 2-2 (A and B), and 2-8 (A to H) PPV aggregates. The electric field is perpendicular to the plane of A. The absorption spectra of 2-1 (dotted line) and 2-2 (dashed line) aggregates are scaled by a factor of 4. Similarly as in Fig. 3, the change of the absorption spectra from one chain to two chains is again very small for higher energy. However, the amplitude of the 2-8 absorption spectrum (solid line) is enhanced, and some of its peaks redshift with respect to those of the 2-2 spectrum. The first peak of 2-1 splits into two in 2-2 and larger splitting is observed in 2-8 PPV (see the inset of Fig. 6). All these effects come from the interchain excitations, which may be observed from the characteristics of corresponding density matrices.

The lowest excited state density matrix for 2-8 PPV ($\omega = 2.95$) is shown in Fig. 7. Complex structure appears in the intrachain component for B, D, F, and H. [Intrachain component for D and F may be observed in Fig. 7(a).] Because the angle between the applied electric field and the chain is neither 0° nor 90°, large σ-π excitation has taken place within a segment and between the neighboring segments in these chains. Since there is no excitation modes near 3 eV for the 2-1 PPV chain, such as A, C, E, and G, the matrix elements within the segment C or E appearing in Fig. 7(a) are thus purely induced by the individual lowest excited states of B, D, F, and H. Dark spots may be observed for the density matrix elements between chain C and other chains like D, E [Fig. 7(a)] or A, B [Fig. 7(b)]. A, B, D, and

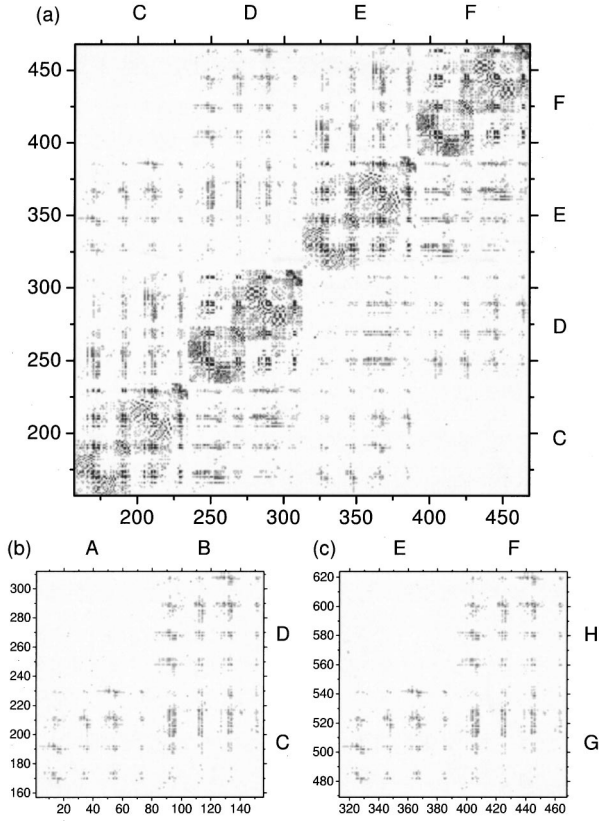

FIG. 7. The lowest excited state ($\omega = 2.95$ eV) density matrix $\delta\overline{\rho}(\omega)$ for 2-8 PPV (Fig. 6). The SMO representation is employed. The absolute vaule of the matrix elements are shown with the gray logarithmic scale (the right-upper corner of Fig. 4). The matrix elements are rescaled by the largest value of $|\delta\overline{\rho}_{ij}|$. (a) Matrix elements for C, D, E, and F. (b) Matrix elements between (A, B) and (C, D). (c) Matrix elements between (E, F) and (G, H). The orbital indices 1–78, 79–156, 157–234, 235–312, 313–390, 391–468, 469–546, and 547–624 belong to A, B, C, D, E, F, and G, respectively.

E are neighbors of C. The matrix elements between chains C and F are very small, which is reflected by a white area in Fig. 7(a). The matrix elements between C and G (or H) are negligibly small. Thus the critical length of the interchain components (about 10 Å) is far much shorter than that of intrachain components (more than 30 Å for a longer chain). The excitations are almost uniform, which is reflected by similarity between Figs. 7(b) and 7(c). The kiltlike pattern is everywhere and this indicates again that the orbitals near segment HOMO or LUMO are important for excitation even for large aggregates.

Ground state charge distribution for 2-8 PPV is shown in Fig. 8(a). Since the total number of electrons on each chain is 78, residual charges are rather small. Comparatively, A and H have a little bit more charges. Induced charges ($-\Sigma_i \delta\rho_{ii}$) on each chain is plotted in [Fig. 8(b)], and fluctuate alternatively among A, B, C, D, E, F, G, and H. This shows clearly that the excitation at $\omega = 2.95$ eV contains interchain charge transfer. Similar features are observed for other excitations.

Figure 9 shows the absorption spectra for 1-chain (dotted line), 2-chain (dashed line), and 8-chain (solid line) PPV aggregates when the electric field $\vec{\mathcal{E}}$ is polarized along the

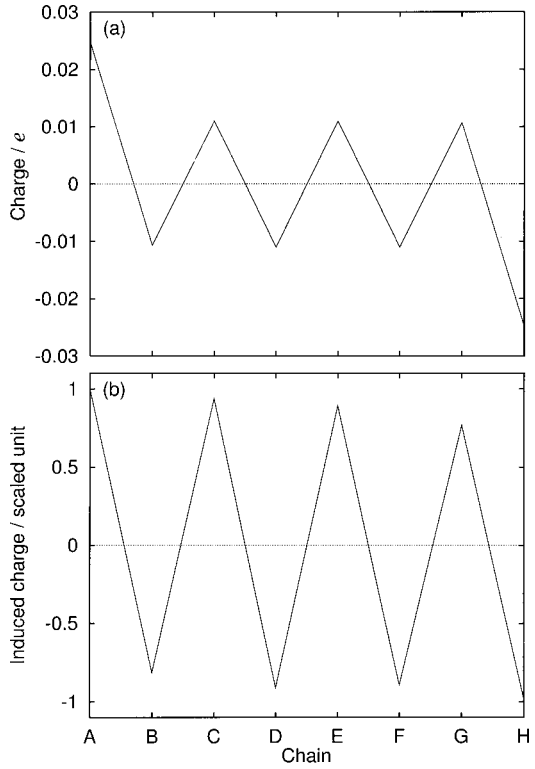

FIG. 8. (a) Ground state charge distribution for 2-8 PPV. (b) Excited state ($\omega = 2.95$ eV) induced charge ($-\Sigma_i \delta\rho_{ii}$) for each chain.

chain axis. Blueshift and suppression of the oscillator strength of the first peak are observed as the aggregate grows. This is consistent with the 2-chain calculation with varying interchain distance,[50] and may be explained as follows. The electron-hole pairs are highly limited within individual chains when $\mathcal{E}$ is polarized along the chain axis. Because of the special packing of PPV chains in our model aggregates, the electron-hole pairs in the adjacent chains have the same phase and thus repel each other. This Coulomb repulsion increases the excitation energy and suppress oscillator strength as well. If adjacent chains are displaced differently so that the phases of electron-hole pairs differ by π, the excitation energy is expected to decrease and the oscillation strength increases due to the Coulomb attraction.

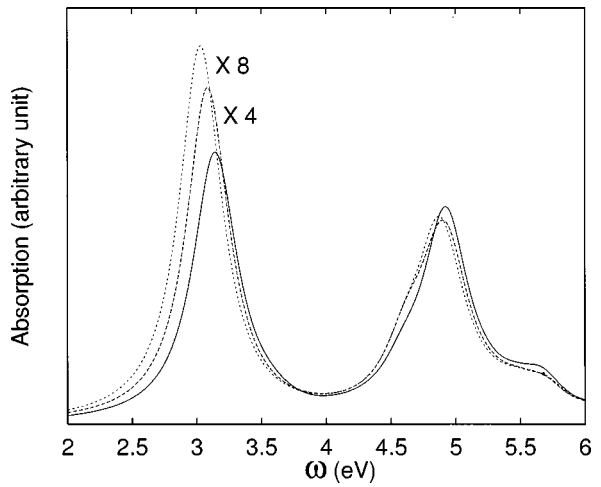

FIG. 9. The absorption spectra for 2-1 (dotted line), 2-2 (dashed line), and 2-8 (solid line) PPV aggregates. Electric field is polarized along the chain axis.

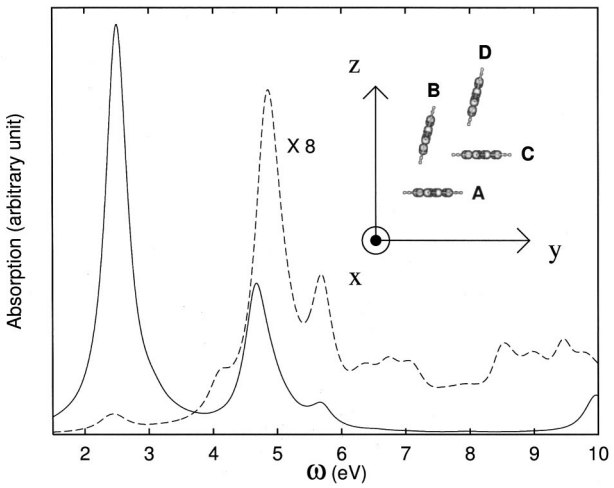

FIG. 10. Absorption spectra for 8-4 PPV aggregate. The electric field is polarized along the chain axis (solid line), or perpendicular to the plane of *A* (dashed line). The amplitude of the dashed line are magnified 8 times. $\gamma = 0.2$ eV.

The absorption spectra of the 8-4 PPV aggregate is plotted in Fig. 10. The electric field is polarized along the chain axis (solid line), or perpendicular to the plane of *A* (dashed line). The first absorption peak is at 2.4 eV while experimentally it is found at 2.5 eV.[58] Compared to the excitations caused by $\vec{\mathcal{E}}$ along the chain, new peaks appear when $\vec{\mathcal{E}}$ is perpendicular to the plane of *A*. This is a clear sign for the anisotropy of PPV crystal. It is thus desirable for experimentalists to investigate the anisotropic effect of dielectric constants in these systems.[33]

IV. DISCUSSION AND CONCLUSION

PPV aggregates are semiconductor, i.e., $\overline{E_g} \neq 0$. However, for metals $\overline{E_g} = 0$, which leads to the divergence in Eq. (9). In this case, we need to use the different expression for C_{ij} including the temperature dependence.[57] More elaboration on Eq. (9) and the choice of the parameter may lead to higher accuracy as well as the efficiency. A better theoretical understanding on the locality of the density matrix is needed.

As we notice that interchain excitations do not alter much the profile of the absorption spectrum. (See also Ref. 59.) However, examining the density matrices reveals considerable contribution from the interchain excitations. Further we observe charge transfer among the different chains in the frequency domain. The contour plot of the density matrix is a much better mean to investigate the dynamics of the intermolecular excitations. As has been shown here and in Refs. 38, and 50 different configurations of the chains will lead to different results. Thus it will be interesting to vary the arrangement of chains in the aggregates and investigate the change of photoexcitation dynamics.

The elongation method[60] uses the localized molecular orbital (LMO)[61] to reduce the computational cost. To calculate the ground state of a one-dimensional system, the con-

stituents are added while portions of LMOs are deleted to keep the computational time constant for each addition. To calculate the excited states, the LMOs are again used and only the electronic excitations involving adjacent LMOs are included to reduce the computational effort. The computational cost of the elongation method scales as $O(N)$ and $O(N^3)$ for the ground and excited states, respectively. The localized orbitals or functions are employed in other ground state linear-scaling methods.[3,6,7,15] Truncation of these localized orbitals leads to $O(N)$ number of Hamiltonian matrix elements and subsequently the linear-scaling of computational cost. Although it is not essential for the linear-scaling calculation, the introduction of the SMO representation reduces further the computational cost of the LDM method.

To summarize, the SMO representation is developed and incorporated into the LDM method. Introducing different cutoff lengths for different pairs of SMOs reduces greatly the LDM/SMO calculation cost. The absorption spectra of various PPV aggregates are calculated via the LDM/SMO method. The interchain excitations are identified convincingly through the examination of the density matrices.

ACKNOWLEDGMENTS

Support from the Hong Kong Research Grant Council (RGC) and the Committee for Research and Conference Grants (CRCG) of the University of Hong Kong is gratefully acknowledged.

[1] W. Yang, Phys. Rev. Lett. **66**, 1438 (1991); W. Yang and T.-S. Lee, J. Chem. Phys. **103**, 5674 (1995).
[2] P. Cortona, Phys. Rev. B **44**, 8454 (1991).
[3] G. Galli and M. Parrinello, Phys. Rev. Lett. **69**, 3547 (1992).
[4] S. Baroni and P. Giannozzi, Europhys. Lett. **17**, 547 (1992).
[5] X.-P. Li, R. W. Nunes, and D. Vanderbilt, Phys. Rev. B **47**, 10891 (1993).
[6] F. Mauri, G. Galli, and R. Car, Phys. Rev. B **47**, 9973 (1993).
[7] P. Ordejón, D. A. Drabold, M. P. Grumbach, and R. M. Martin, Phys. Rev. B **48**, 14646 (1993).
[8] W. Kohn, Chem. Phys. Lett. **208**, 167 (1993).
[9] D. A. Drabold and O. F. Sankey, Phys. Rev. Lett. **70**, 3631 (1993).
[10] A. Gibson, R. Haydock, and J. P. LaFemina, Phys. Rev. B **47**, 9229 (1993).
[11] M. Aoki, Phys. Rev. Lett. **71**, 3842 (1993).
[12] E. B. Stechel, A. P. Williams, and P. J. Feibelman, Phys. Rev. B **49**, 10088 (1994).
[13] S. Goedecker and L. Colombo, Phys. Rev. Lett. **73**, 122 (1994).
[14] J. P. Stewart, Int. J. Quantum Chem. **58**, 133 (1996).
[15] E. Hernández and M. J. Gillan, Phys. Rev. B **51**, 10157 (1995); E. Hernández, M. J. Gillan, and C. M. Goringe, *ibid.* **55**, 13485 (1997).
[16] M. C. Strain, G. E. Scuseria, and M. J. Frisch, Science **271**, 51 (1996).
[17] S. L. Dixon and K. M. Merz, Jr., J. Chem. Phys. **104**, 6643 (1996).
[18] E. Schwegler, M. Challacombe, and M. Head-Gordon, J. Chem. Phys. **106**, 9708 (1997).
[19] W. Yang, Phys. Rev. B **56**, 9294 (1997).
[20] For review, see S. Goedecker, Rev. Mod. Phys. **71**, 1085 (1999).
[21] S. Yokojima and G. H. Chen, Phys. Rev. B **59**, 7259 (1999).
[22] S. Yokojima and G. H. Chen, Chem. Phys. Lett. **292**, 379 (1998).
[23] A. Takahashi and S. Mukamel, J. Chem. Phys. **100**, 2366 (1994).
[24] H. Fukutome, J. Mol. Struct.: THEOCHEM **188**, 337 (1989).
[25] Z. G. Soos, S. Ramasesha, D. S. Galvão, and S. Etemad, Phys. Rev. B **47**, 1742 (1993).
[26] J. Del Bene and H. H. Jaffé, J. Chem. Phys. **48**, 1807 (1968); **48**, 4050 (1968).
[27] J. J. P. Stewart, J. Comput. Chem. **10**, 209 (1989); **10**, 221 (1989).
[28] W. Z. Liang, X. J. Wang, S. Yokojima, and G. H. Chen (in preparation).
[29] W. Z. Liang, S. Yokojima, and G. H. Chen, J. Chem. Phys. **110**, 1844 (1999).
[30] S. Yokojima and G. H. Chen, Chem. Phys. Lett. **300**, 540 (1999).
[31] S. Yokojima, D. H. Zhou, and G. H. Chen, Chem. Phys. Lett. **302**, 495 (1999).
[32] W. Z. Liang, S. Yokojima, D. H. Zhou, and G. H. Chen, J. Phys. Chem. (in press).
[33] R. H. Friend, D. D. C. Bradley, and P. D. Townsend, J. Phys. D: Appl. Phys. **20**, 1367 (1987).
[34] U. Lemmer *et al.*, Chem. Phys. Lett. **240**, 373 (1995).
[35] I. D. W. Samuel *et al.*, Chem. Phys. Lett. **213**, 472 (1993).
[36] I. D. W. Samuel, G. Rumbles, and C. J. Collison, Phys. Rev. B **52**, 11573 (1995).
[37] I. D. W. Samuel *et al.*, Chem. Phys. **227**, 75 (1998).
[38] P. Gomes da Costa, R. G. Dandrea, and E. M. Conwell, Phys. Rev. B **47**, 1800 (1993).
[39] H. A. Mizes and E. M. Conwell, Phys. Rev. B **50**, 11243 (1994).
[40] E. M. Conwell, Phys. Rev. B **57**, 14200 (1998).
[41] W. Graupner *et al.*, Phys. Rev. Lett. **77**, 2033 (1996).
[42] J. Grüner *et al.*, Adv. Mater. **6**, 748 (1994).
[43] S. A. Jenekhe and J. A. Osaheni, Science **265**, 765 (1994).
[44] M. Yan *et al.*, Phys. Rev. Lett. **72**, 1104 (1994).
[45] E. S. Maniloff, V. I. Klimov, and D. W. McBranch, Phys. Rev. B **56**, 1876 (1997).
[46] U. Rauscher, H. Bässler, D. D. C. Bradley, and M. Hennecke, Phys. Rev. B **42**, 9830 (1990).
[47] R. J. O. M. Hoofman, M. P. de Haas, L. D. A. Siebbeles, and J. M. Warman, Nature (London) **392**, 54 (1998).
[48] E. L. Frankevich *et al.*, Phys. Rev. B **46**, 9320 (1992).
[49] G. H. Gelinck, J. M. Warman, and E. G. J. Staring, J. Phys. Chem. **100**, 5485 (1996).
[50] T. Wagersreiter and S. Mukamel, Chem. Phys. **210**, 171 (1996).
[51] J. H. Burroughes *et al.*, Nature (London) **347**, 539 (1990).
[52] G. Gustafsson *et al.*, Nature (London) **357**, 477 (1992).
[53] K. Nishimoto and N. Mataga, Z. Phys. Chem., Neue Folge **12**, 335 (1957).
[54] S. Yokojima, T. Meier, and S. Mukamel, J. Chem. Phys. **106**, 3837 (1997).
[55] P. Ring and P. Schuck, *The Nuclear Many-Body Problem* (Springer, New York, 1980).
[56] G. H. Chen and S. Mukamel, J. Am. Chem. Soc. **117**, 4945 (1995).
[57] S. Ismail-Beigi and T. A. Arias, Phys. Rev. Lett. **82**, 2127 (1999).
[58] D. A. Halliday *et al.*, Synth. Met. **55–57**, 954 (1993).
[59] S. Yokojima, X. J. Wang, and G. H. Chen, Thin Solid Films (in press).
[60] A. Imamura, Y. Aoki, and K. Maekawa, J. Chem. Phys. **95**, 5419 (1991); Y. Kurihara, Y. Aoki, and A. Imamura, *ibid.* **107**, 3569 (1997).
[61] V. Magnasco and A. Perico, J. Chem. Phys. **47**, 971 (1967); **48**, 800 (1968).